Journal of Power Sources 222 (2013) 21–31

Contents lists available at SciVerse ScienceDirect

Journal of Power Sources

journal homepage: www.elsevier.com/locate/jpowsour

Vanadium oxides–reduced graphene oxide composite for lithium-ion batteries and supercapacitors with improved electrochemical performance

Hongbin Zhao, Lanying Pan, Siyi Xing, Jun Luo, Jiaqiang Xu*

College of Science, Shanghai University, 99 Shangda Road, Shanghai 200444, China

HIGHLIGHTS

- Vanadium oxides–rGO were synthesized at first time by hydrothermal reduction-heat treatment.
- Enhanced stable performance for Lithium-ion batteries and supercapacitors was obtained.
- The uniform coating of graphene ensures good close electrical contact and cycling performance.

GRAPHICAL ABSTRACT

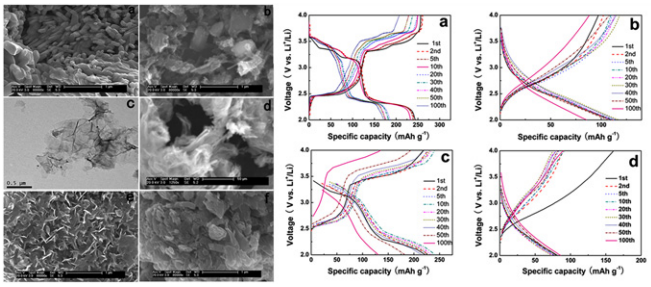

ARTICLE INFO

Article history:
Received 31 January 2012
Received in revised form
9 August 2012
Accepted 13 August 2012
Available online 13 September 2012

Keywords:
Vanadium oxides
Cathode
Rechargeable battery
Supercapacitor
Reduced graphene oxide

ABSTRACT

A facile approach to the surface reduced graphene oxide (rGO) modification of micro-nano structured vanadium oxides composites are developed as cathode materials of lithium ions batteries (LIBs) and supercapacitors (SCPs) for the first time. The as-prepared V_2O_5–rGO and VO_2–rGO composites exhibit remarkably enhanced cycling performance when being used as cathode materials in LIBs and SCPs, respectively. The uniform coating of graphene around the surface of vanadium oxides ensures good close electrical contact, therefore higher specific capacity and enhanced cycling performance than pure VO_2 and V_2O_5 electrodes. Meanwhile, the cycling performance enhancement and capacity decay mechanism are presented, which is not only important to design electrode materials in LIBs and SCPs, but also extendable to the design and fabrication of other functional materials for energy storage and transfer systems.

1. Introduction

The storage of energy through electrochemical reactions is a crucial technology for portable power needs. The proliferation of personal electronics and commercialization of electric and hybrid electric vehicles have popularized the needs for rechargeable and portable power sources [1,2].

Many transition metal oxides nanoparticles have been employed as lithium ions batteries (LIBs) electrode materials to improve cell properties in several ways [3–6]. Usually small diameter particles have large surface-to-volume ratios, short lithium diffusion lengths. Therefore, the greater available surface area and reduction of particle sizes from micrometers to nanometers result in orders of magnitude increase in lithium insertion and discharging kinetics. While the small diameter particles also are thermodynamically unstable and ease to aggregate after longtime charge/discharge process. So some scientists recommended the micro-nano structured materials or hybrid to get more stabled electrochemical performance [7–9].

* Corresponding author. Tel./fax: +86 (0)21 66132406.
E-mail addresses: hongbinzhao@shu.edu.cn (H. Zhao), xujiaqiang@shu.edu.cn, xujiaqiang@zzuli.edu.cn (J. Xu).

0378-7753/$ – see front matter © 2012 Elsevier B.V. All rights reserved.
http://dx.doi.org/10.1016/j.jpowsour.2012.08.036

Vanadium oxides have been researched for several decades and are widely used as cathode material for LIBs and supercapacitors (SCPs) [10–14]. Theoretically, the specific capacities for V_2O_5 as cathode and anode are 290 mAh g^{-1} and 1471 mAh g^{-1}, respectively, thus to be a promising electrode material. Unfortunately, the volume expansion and structure collapse of V_2O_5 or unstable intermediates formation during the longtime charge/discharge processes seriously destroyed its initial structure, even separated from conductive carbon materials. As for VO_2, it is difficult to synthesize by high temperature procedures as it tends to transform when the temperature is higher than 300 °C and the thermodynamically more stable rutile VO_2 formed, which is not an attractive cathode [15]. Asim et al. tried to synthesize VO_2 in hydrothermal environment with cetyltrimethyl ammonium bromide (CTAB) as reductant and template at low temperature [16]. As a cathode material, the lithium storage and capacitor performance of VO_2 also were studied in aqueous and non-aqueous electrolytes.

To improve the electrochemical performance of vanadium oxides, many efforts have been made to synthesize V_2O_5 with different morphology and structure, such as nanorods [16], nanofibers [17], nanotubes and nanowires [18–20]. Takahashi [14] et al. discovered that nanorods grown by electrochemical deposition had five times greater current density than substrates with poorer crystallinity synthesized by a sol–gel method and the crystallinity of V_2O_5 nanorods aided Li intercalation. $V_2O_5.nH_2O$ also was suggested to be even more active for lithium incorporation, and $Ni@V_2O_5.nH_2O$ core shell nanowire arrays showed 10 times greater current density than the crystal nanorods [21]. Conflictingly, Cao [22] et al. found that amorphous V_2O_5 nanotube arrays also showed promising specific capacities of about 300 mAh g^{-1}, but degraded by cycling to 160 mAh g^{-1}. Chan et al. determined that the diffusion of lithium in V_2O_5 was up to 1000 times faster in nanoribbons than in bulk. Another potential approach to overcome these shortcomings of vanadium pentoxide is surface modification with carbon materials and conducting polymers. V_2O_5@PPy [23–26] or V_2O_5/PANI [27] hybrid cathodes have been synthesized to improve the cycling performance of vanadium oxides cathodes. V_2O_5/C composite also has been reported by Stojković and Cai [28,29] and the electrochemical performance were studied.

Graphene, the name given to a flat monolayer of carbon atoms tightly packed into a two-dimensional (2D) honeycomb lattice, exhibits many unusual and intriguing properties in magnetic, electronic, photonic fields et al. In particular, its superior electrical conductivities, high surface areas and chemical tolerance intrigue great interest in energy storage technologies, such as LIBs [8,30,31] and SCPs [32–34]. Additionally, graphene has been used as conductive support material to modify the electrochemical performance of electrode materials. Till now, metal oxide (CuO [35–36], NiO [9,37], Mn_3O_4 [38], TiO_2 [39], SnO_2 [40], Co_3O_4 [41–42])/graphene composites have been synthesized and used as anode materials in LIBs and SCPs. Graphene modified $LiFePO_4$ as cathode is reported with more stable electrochemical performance [43]. To the best of our knowledge, there are few reports devoted to the synthesis of vanadium oxides–graphene composites.

In present work, in order to improve the electronic conductivity and electrochemical performance of vanadium oxides electrodes during the charge/discharge process, the reduced graphene oxide (rGO) was employed to modify V_2O_5 and VO_2 electrode materials by an in-situ chemical synthesis approach. A synergetic effect between vanadium oxides and rGO was wished to improve the capacity and cycling performance of V_2O_5 and VO_2 electrode. The reversible capacity and improved cycling performances of the V_2O_5–rGO and VO_2–rGO composites in comparison with the pristine vanadium oxides were evaluated. We expected that in-situ coating technique of rGO on the surface of metal oxides could be applicable to design other cathode materials with high conductivity and good cycling performance.

2. Experimental section

2.1. Preparation of graphene oxide (GO) and reduced graphene oxide (rGO)

GO was prepared by oxidizing natural flake graphite (about 300 meshes, Qingdao Tianhe Graphite Co., Ltd. China) with a procedure following traditional modified Hummers method that produced mostly several layers GO [44]. Briefly, the graphite was first treated with conc. H_2SO_4, P_2O_5, and $K_2S_2O_8$. After filtered and washed with DDI water for several times, the suspension was dried at 45 °C for 24 h, the pretreated graphite was obtained. The pretreated flake graphite was further oxidized to graphite oxide by three step oxidation method in ice bath, at 35 °C and 98 °C. The solid was re-suspended in conc. H_2SO_4 and further oxidized by $KMnO_4$. Afterward, 3 wt% H_2O_2 was added to change residual $KMnO_4$ to Mn^{2+} in conc. H_2SO_4 solution, thus a thick and brownish yellow suspension was obtained. The graphite oxide suspension was washed with 10% HCl aqueous solution, then repeatedly with DDI (distilled, deionized) water until pH is 7, and dried at 40 °C for 24 h. Finally, graphite oxide was dispersed in DDI water with GO concentration of 1 mg mL^{-1} by ultrasonic.

The pure rGO was prepared by pyrolysis of graphite oxide in quartz tube furnace at 550 °C for 2 h with the protection of high pure Ar.

2.2. Fabrication of micro-nanosized vanadium oxides and vanadium oxides–rGO

0.9117 g commercial V_2O_5 (several micrometers) and 2.191 g cetyltrimethyl ammonium bromide (CTAB) were dispersed in 40 mL DDI water or rGO (1 mg mL^{-1}) aqueous solution, then kept vigorously stirring for 3 h in room temperature. The obtained yellow slurry was removed to 50 mL Teflon kettle, and the volume of slurry was about 80%–90% of the total volume. Then the kettle was kept at 190 °C for 48 h. After cooled to room temperature, the precipitate was obtained in the bottom of kettle. Washed by ethanol and DDI water for several times to remove impurities, the filter cake was dried at 50 °C for 24 h and the black precursor was obtained. Followed, some of the black precursor was heated in furnace at 500 °C for 2 h and V_2O_5 or V_2O_5–rGO was obtained. As comparison, other precursor was heated under a nitrogen atmosphere at 550 °C for 2 h to remove the organic impurities by heating rate of 5 °C min^{-1} and the obtained powder was VO_2 or VO_2–rGO hybrid material.

2.3. Physicochemical characterization

The crystalline phase of as synthesized vanadium oxides and their rGO modification composites were analyzed by a powder X-ray diffractometer (XRD, Rigaku DLMAX-2550 V) using Cu Kα (λ = 1.54,056 Å) radiation between 10° and 90° at a scan rate of 0.01° s^{-1}. X-ray photoelectron spectroscopy (XPS) analysis was carried out on a PHI-5000C ESCA system (Perkin Elmer). The binding energies were calibrated with reference to C_{1s} at 284.60 eV. The data were imported into XPSPEAK 4.1 software for curve-fitting. The morphology of cathode materials was characterized by scanning electron microscope (SEM, JEOL JSM-6700F) and transmission electron microscope (TEM, JEM-2010F). Raman spectra were obtained by a Renishaw inVia plus laser Raman spectrometer with a laser wavelength of 488 nm and a spot size of 0.5 mm. Inductively Coupled Plasma Atomic Emission

Spectrometer (ICP-AES) was used to quantify the content of vanadium element in the vanadium oxide–rGO composites after the samples were dissolved in diluted hydrochloric acid.

2.4. Electrochemical characterization

Vanadium oxides electrodes were fabricated by coating an NMP-based slurry with a mixture of 80.0 wt% of active materials, 10 wt% of polyvinylidene fluoride (PVDF) binder and 10 wt% of carbon black on an aluminum current collector. After dried at 80 °C in vacuum oven for 12 h, then it was cut into a 9 mm diameter discs as cathode. A solution of $LiPF_6$ in EC/DMC/DEC (1: 1: 1 in weight) (Guotaihuarong LTD., Zhangjiagang, China) was used as electrolyte. The separator (Celgard 2400, microporous polypropylene membrane) was purchased from Celgard Inc. The electrochemical performances were evaluated with CR2016 coin-type cells, which were fabricated with the prepared cathodes, metallic lithium anodes and electrolyte in an argon-filled glovebox (Universal series, Mikrouna). The cell performance such as discharge capacity, C-rate capability, and cyclability was examined using battery test equipment (CT2001A, LAND, Wuhan, China). The charge/discharge capacities and C-rate capability were evaluated by varying the charge/discharge current (i.e., discharge C-rates) from 20 mA g^{-1} to 100 mA g^{-1} under a voltage range of 2.0–4.0 V. Cyclic voltammetry (CV) and AC impedance measurement of the coin-type cells were carried out on Solartron 1287 electrochemical interface +1255B frequency analyzer. CV curves were obtained between 2 and 4 V vs. Li^+/Li with scan speed of 0.1 mV s^{-1}. Electrochemical impedance spectrum (EIS) was obtained over a frequency range of 10^{-2}–10^6 Hz.

3. Results and discussion

Prior to evaluating cell performance, the surface morphology of rGO, as synthesized vanadium oxides and vanadium oxides–rGO composites was comprehensively characterized. Fig. 1 demonstrates that the obtained V_2O_5 rods with 200 nm in width and 700–800 nm in length were obtained after the precursor was treated in O_2 at 550 °C for 2 h (Fig. 1-a). The interface of V_2O_5–rGO composite became obscure when rGO coated on the surface of V_2O_5 (Fig. 1-b) and similar morphology and dimensional scale was kept well. Intimate contact with each other in the micro-nanoscale was formed. As a reference, the SEM and TEM images of rGO sheets obtained by graphite chemical oxidation were supplied with a several-layer structure (Fig. 1-c and d). The obtained VO_2 was uniform lamellar 3D structure with 20 nm in thickness (Fig. 1-e). The formation of lamellar VO_2 should be attributed to the CTAB, which not only was used as a reductant but also as a template. Comparison with pure VO_2, obvious structural aggregation was observed in VO_2–rGO (Fig. 1-f) because of the homogenous dispersion between VO_2 and rGO. Fig. 2 showed HRTEM images of VO_2–rGO and V_2O_5–rGO. The thicknesses of rGO layer were observed on the surface of V_2O_5 and VO_2 is about 7 nm and 3 nm, respectively. This result indicated a homogenously coating of rGO.

Schematic illustrations of this nanoarchitectured rGO wrapping layer formed onto the V_2O_5 and VO_2 surface and its function as an

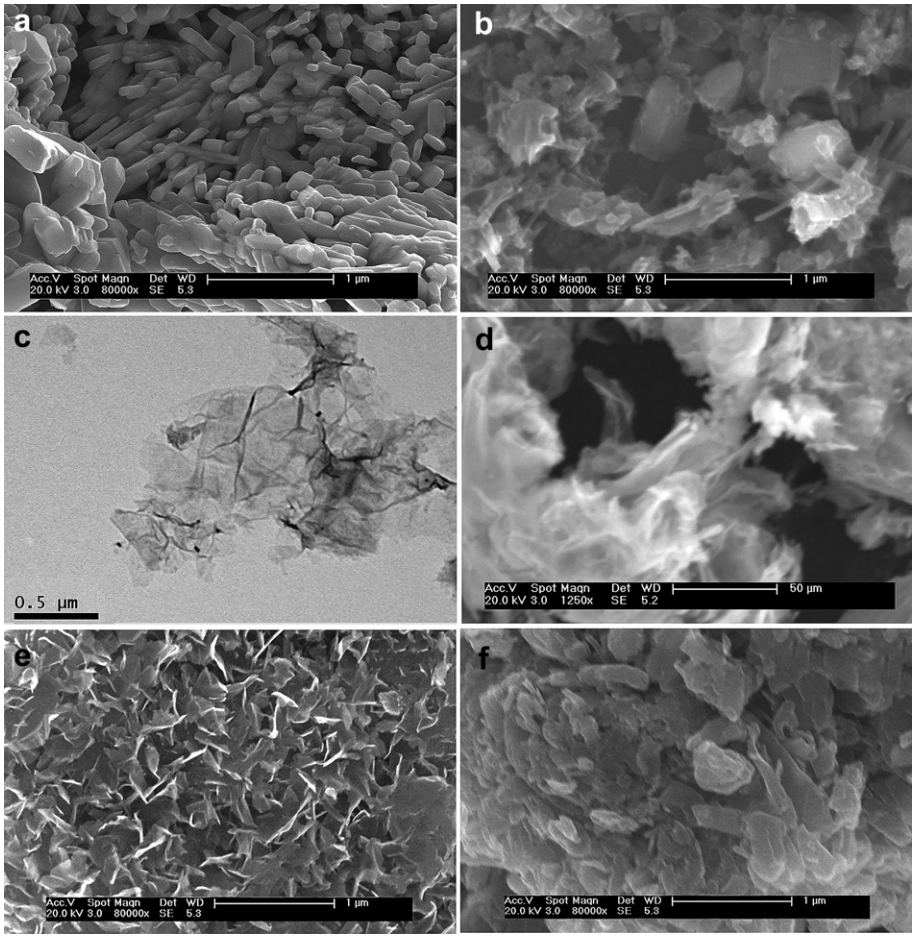

Fig. 1. SEM and TEM images of V_2O_5 (a), V_2O_5–rGO (b), rGO (c–d), VO_2 (e) and VO_2–rGO (f).

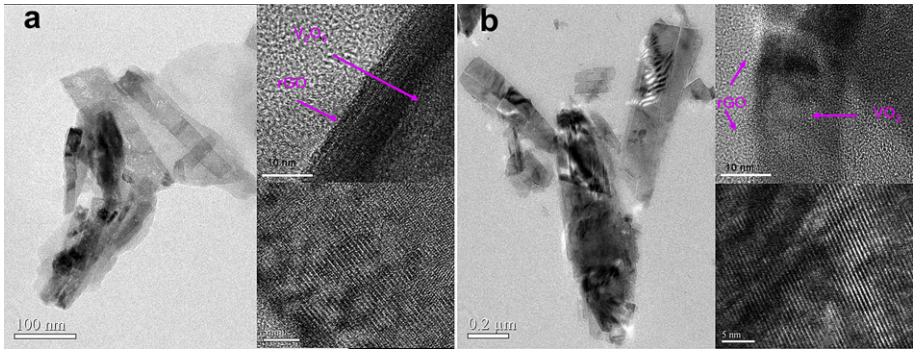

Fig. 2. HRTEM images of V_2O_5–rGO (a) and VO_2–rGO (b).

electronic conductive protection skin to suppress the undesired interfacial reactions are provided in Fig. 3. GO with abundant function groups, including hydroxyl, carboxyl and carbonyl, was easy for GO uniform attachment on the surface of V_2O_5 via electrochemical bonds. Therefore, homogeneous carbon layer coating enhance the conductivity of electrode with less weight increase. CTAB was employed as reductant and template in the hydrothermal process and lamellar VO_2 and rod-like V_2O_5 was successfully synthesized in different atmosphere, respectively.

XRD patterns (Fig. 4-a) of vanadium oxides–rGO composites were compared with those of the pristine vanadium oxides. It is confirmed that V_2O_5 was successfully reduced to VO_2 though hydrothermal reduction with CTAB as a reductant. After the precursor was heated in O_2 or N_2 atmosphere, micro-nanoscaled V_2O_5 and VO_2 were obtained, respectively. Indexing by standard diffraction card (PDF#41-1426 and PDF#44-0252), XRD patterns of pure VO_2 and V_2O_5 was identical to that of r-VO_2 and α-V_2O_5, respectively. In case of precursors obtained with GO as dispersion, α-V_2O_5 and VO_2 were synthesized after precursors were heated at 550 °C for 2 h and the diffraction peaks of rGO were very weak for its amorphous phase and low concentrate in the hybrid cathodes. After Jade software refine, the crystallinity of VO_2–rGO and V_2O_5–rGO is 94.5% and 91.7%, respectively. This result indicated that rGO modified vanadium oxides does not change their crystal form and V_2O_5 and VO_2 with high crystallinity and uniformity were obtained.

ICP-AES results showed that V_2O_5 and VO_2 in the vanadium oxides–rGO was 92% and 84%, respectively. The estimated weight fraction of V_2O_5 and VO_2 for the conditions to prepare their rGO composites is 96.8% and 94.7%, respectively. This theoretic weight fraction is larger than that of the ICP-AES result. The reason maybe

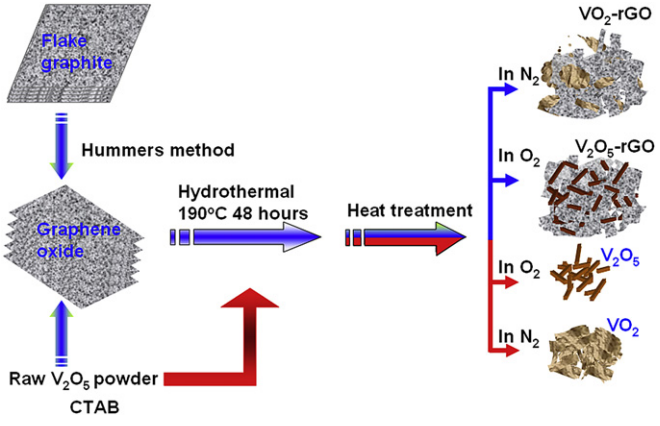

Fig. 3. Scheme of synthesizing V_2O_5–rGO and VO_2–rGO cathode materials.

is that CTAB was not removed completely, which cause the weight fractions of vanadium oxides decrease in the composites. Also, the GO solution is weak acidic, and part of V_2O_5 can react with H^+ and formed soluble VO^{2+}, in further loss after washing [45].

XPS spectra (Fig. 4-b) showed that the survey spectrum of as prepared V_2O_5–rGO and VO_2–rGO , and the insert is V2p core-level spectrum with precise test. The V2p core-level spectrum illustrates that two peaks at 516.4 and 523.5 eV are attributed to the spin-orbit splitting of the components, $V_{2p3/2}$ and $V_{2p1/2}$, which is the characteristic of vanadium in the +4 oxidation state in the bulk. Two peaks at 517.7 and 524.8 eV of V_2O_5–rGO are the characteristic of vanadium in the +5 oxidation states in the bulk [49], which confirmed that with rGO as carbon coating layer, the +5 oxidation state of vanadium stable exist in V_2O_5 and V_2O_5–GO. The difference in binding energy (Δ) of O_{1s} and $V_{2p3/2}$ for V_2O_5 and VO_2 is 13.6 eV and 12.7 eV, respectively, means different vanadium oxidation state in vanadium oxides and theirs composites. These results are corresponding to most of literature [46–49].

Raman spectroscopy shown in Fig. 5 confirmed that the rGO obtained by high temperature pyrolysis method had large area ratio of G band to D band, which represented high graphited degree and low chemical structure faults in rGO nanosheets. The G band and D band represent the sp2 and sp3 hybridization of carbon atom on the carbon materials, respectively. Usually, sp2 hybridization mean the C=C structure of carbon, while sp3 hybridization mean that part of the C=C structure is destroyed. The area ratio of G band to D band is used to evaluate the ratio of the C=C structure remained. In this work, the area ratio of sp3 to sp2 for GO, rGO, VO_2–rGO and V_2O_5/rGO is 0.76, 0.89, 0.88 and 0.85, respectively. An improved graphited rGO on the surface of V_2O_5 and VO_2 is obtained.

In case of V_2O_5–rGO and its precursors, the D and G band of rGO still were obvious and V_2O_5 adsorption peaks could be found at Raman shift of 994 nm^{-1}, 705 nm^{-1} and 515 nm^{-1}, which indicated a perfect composite action between vanadium oxides and rGO nanosheets. As for VO_2–rGO composite, besides of high D and G bond of rGO, which represented low faults and high graphited degree of rGO, one peak at 640 nm^{-1} representing Raman shift of VO_2.

BET adsorption isotherms shown in Fig. 6 were used to study the change of specific surface of vanadium oxides. The BET surface area of rGO, V_2O_5, VO_2, VO_2–rGO and V_2O_5–rGO is about 345 $cm^2\ g^{-1}$, 17 $cm^2\ g^{-1}$, 8 $cm^2\ g^{-1}$, 35 $cm^2\ g^{-1}$ and 64 $cm^2\ g^{-1}$, respectively. In this view, rGO obviously improved the specific surface of V_2O_5 and VO_2.

Electrochemical properties of as synthesized vanadium oxides-based electrodes for Li-ion storage performance were evaluated using galvanostatic charge/discharge. Galvanostatic cycling tests showed us the detailed description about the variation of the specific capacity versus voltage (vs. Li^+/Li) as indicated in Fig. 7. Two lithium ions were inserted into the crystalline of V_2O_5 and V_2O_5–rGO step by step and three obvious plateaus were observed at

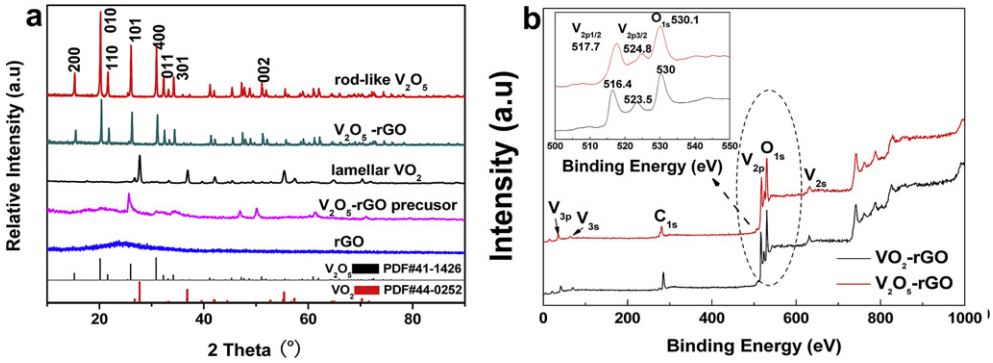

Fig. 4. XRD patterns (a) and XPS spectra (b) of VO_2, V_2O_5, rGO and their complexes.

around 2.50/2.35 V, 3.30/3.25 V, 3.60/3.50 V in the initial charge/discharge cycle, which is corresponding to 1.0 Li^+ (Eq. 3), 0.5 Li^+ (Eq. (2)) and 0.5 Li^+ (Eq. (1)) insertion/delithiation, respectively. By calculating the number of Li^+ insertion/delithiation according to the experimental data (Fig. 7), about 65, 60 and 122 mAh g^{-1} capacity in different steps, which corresponding to 0.45, 0.44 and 0.86 Li^+ insertion/delithiation. The initial charge capacity of V_2O_5 and V_2O_5–rGO cathodes was 250 mAh g^{-1} and 235 mAh g^{-1}, respectively. About 86% and 81% of theoretical lithium storage capacity was achieved, which indicated promising application as cathode of LIBs. In case of the charge/discharge curves with VO_2 and VO_2–rGO as cathode, the initial discharge capacity of VO_2 and VO_2–rGO is 85 mAh g^{-1} and 110 mAh g^{-1}, respectively. No obvious charge/discharge plateau but an asymmetrical capacitor behavior was observed, implying promising capacitive performance rather than lithium storage.

The charge/discharge curves of as synthesized V_2O_5 and V_2O_5–rGO cathodes showed a multi-step process due to their structural changes upon the two Li^+ ions insertion/extraction process. The electrochemical reaction between vanadium oxides and metal lithium can be described as followed [13]:

$$V_2O_5 + 0.5\ Li^+ + 0.5e \leftrightarrow Li_{0.5}V_2O_5 \quad (1)$$

$$Li_{0.5}V_2O_5 + 0.5\ Li^+ + 0.5e \leftrightarrow LiV_2O_5 \quad (2)$$

$$LiV_2O_5 + 1\ Li^+ + 1e \leftrightarrow Li_2V_2O_5 \quad (3)$$

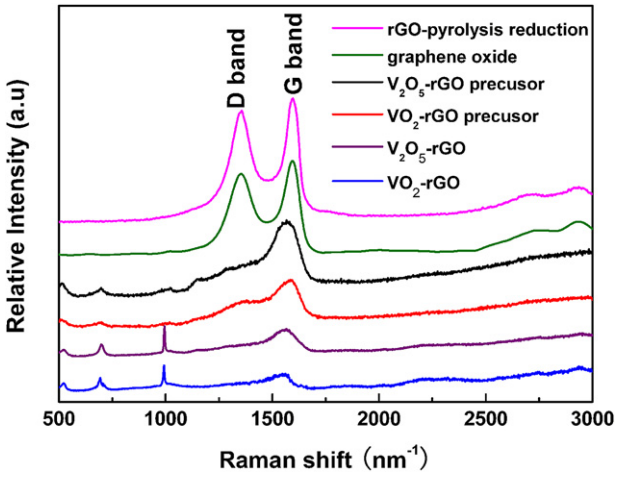

Fig. 5. Raman spectroscopy of GO, rGO, VO_2–rGO and V_2O_5–rGO composites.

In case of VO_2, one Li^+ insertion/extraction theoretically occurred in the voltage range from 2 V to 4 V (Eq. (4)), but we cannot find an obvious plateau in the charge/discharge process. This indicated a capacitor characteristic other than a battery.

$$VO_2 + 1\ Li^+ + 1e \leftrightarrow LiVO_2 \quad (4)$$

The cycling stability of vanadium oxide electrodes were evaluated by 100 cycles charge/discharge process. Fig. 8 showed the curves of charge/discharge capacity versus the cycle number for the electrodes made of VO_2, V_2O_5 and rGO modified vanadium oxide with charge/discharge current density of 20 mA g^{-1} at 25 °C. Obviously, the discharge specific capacity of V_2O_5–rGO still achieved at about 171 mAh g^{-1} after 100 cycles, about 1.3 times higher than that of pure V_2O_5. The discharge specific capacity of VO_2–rGO decreased from the initial capacity of 115 mAh g^{-1} to 85 mAh g^{-1}. In case of pure VO_2, only 83 mAh g^{-1} was kept after 100 cycles. This result indicated improved cycling stability of rGO modified vanadium oxide electrodes.

Distinctly, the rGO coating significantly improved the cycling performance of vanadium oxide electrode. The structure collapse of vanadium oxides was restrained with rGO as elastic protecting shell. Also enhanced conductivity of the electrodes was expected by coating rGO layer on the surface of vanadium oxides. However, slow decay of capacity after 40 cycles was still observed on all the researched electrodes, which indicated the structure collapse or irreversible phase transformation of active materials during repeatedly charge/discharge process.

The C-rates performance of as-prepared cathode materials shown in Fig. 9 also confirmed that by coating rGO layer on the surface of vanadium oxides cathode materials, the reversible capacity of V_2O_5–rGO and VO_2–rGO improved after recovered to 93% and 96% of initial capacity. Obviously, only 88% and 83% of initial capacity for V_2O_5 and VO_2 was observed when C-rate descended from 0.1 mA to 0.02 mA. This result indicated improved C-rates performance of vanadium oxide electrodes.

As there is close electrical contact between rGO and vanadium oxides at the micro-nanoscaled level around the outside of vanadium oxides, the kinetics of Li insertion/extraction and the Li storage performance can be expected to be improved in the vanadium oxides–rGO composites over those of conventional materials. Therefore, the kinetic mechanism of vanadium oxides electrodes were discussed by CV technique in the voltage window from 2.0 V to 4.0 V vs. Li^+/Li. As clearly shown in Fig. 10, more than three pairs of oxidation/reduction reversible peak for pure V_2O_5 electrode in the initial scan were observed at 3.4, 3.2 and 2.7 V vs. Li^+/Li, which indicated a multi-step lithiation/delithiation process, and the corresponding phases were transformed from α-V_2O_5 to ε-$Li_{0.5}V_2O_5$ (3.31 V), δ-LiV_2O_5 (3.12 V) and γ-$Li_2V_2O_5$ (2.17 V), consecutively

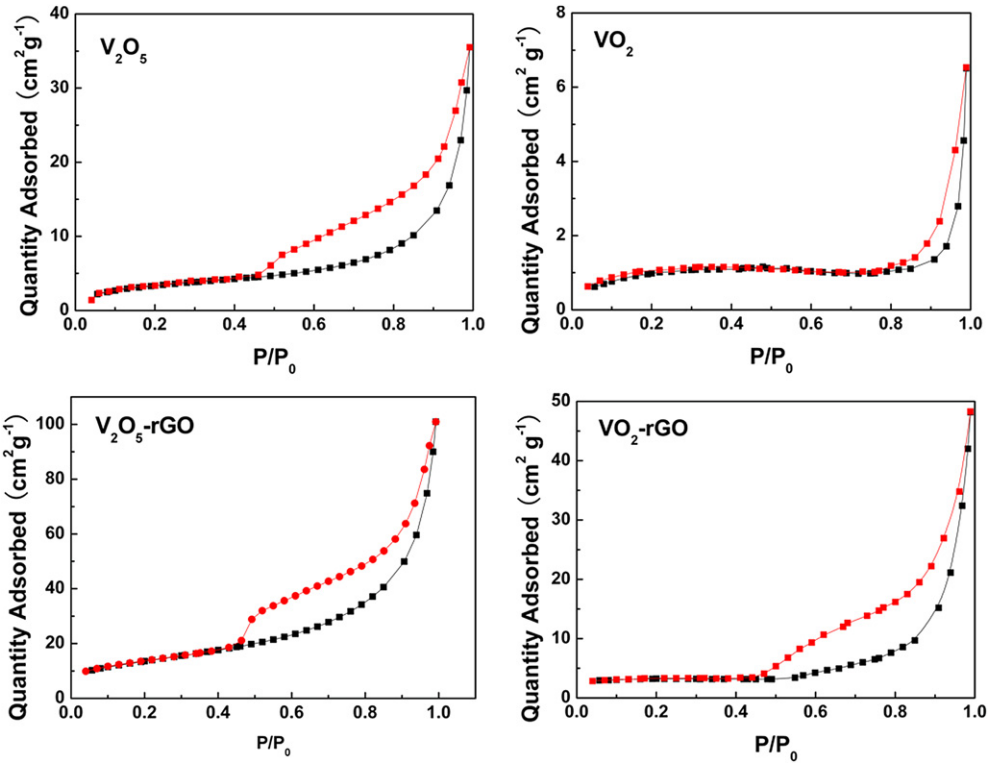

Fig. 6. BET adsorption isotherm of V_2O_5, VO_2 and their rGO composites.

(Eqs. (1)–(3)) [13]. This result was corresponding to that of the initial charge/discharge curves (Fig. 7). In case of VO_2 electrode, wide flat oxidation/reduction peaks were observed at the first two cycles, while the oxidation/reduction peak became blurred after three CV cycles, which maybe caused by the active process of CV. Though the mechanism for the charge storage of VO_2 is as described of Eq. (4), the charge/discharge plateaus are not obvious at the potential range from 2 V to 4 V, and cannot discharge with stable

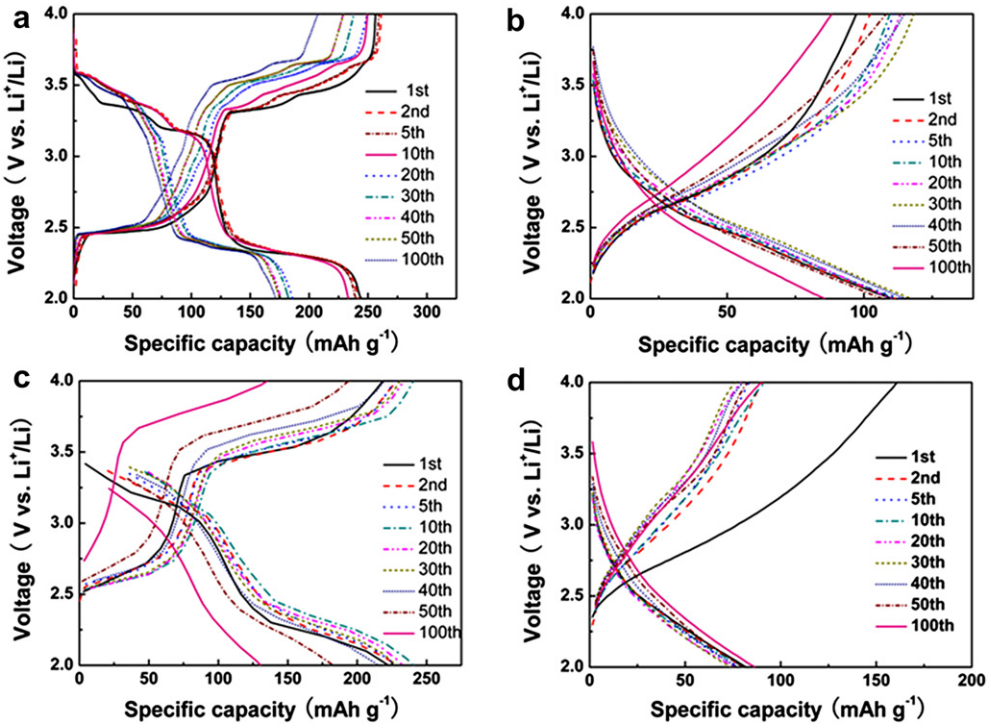

Fig. 7. Charge/discharge curves of the vanadium oxides and vanadium oxides–rGO cathodes with current density of 20 mA g^{-1}. a: V_2O_5–rGO, b: VO_2–rGO, c: V_2O_5, d: VO_2.

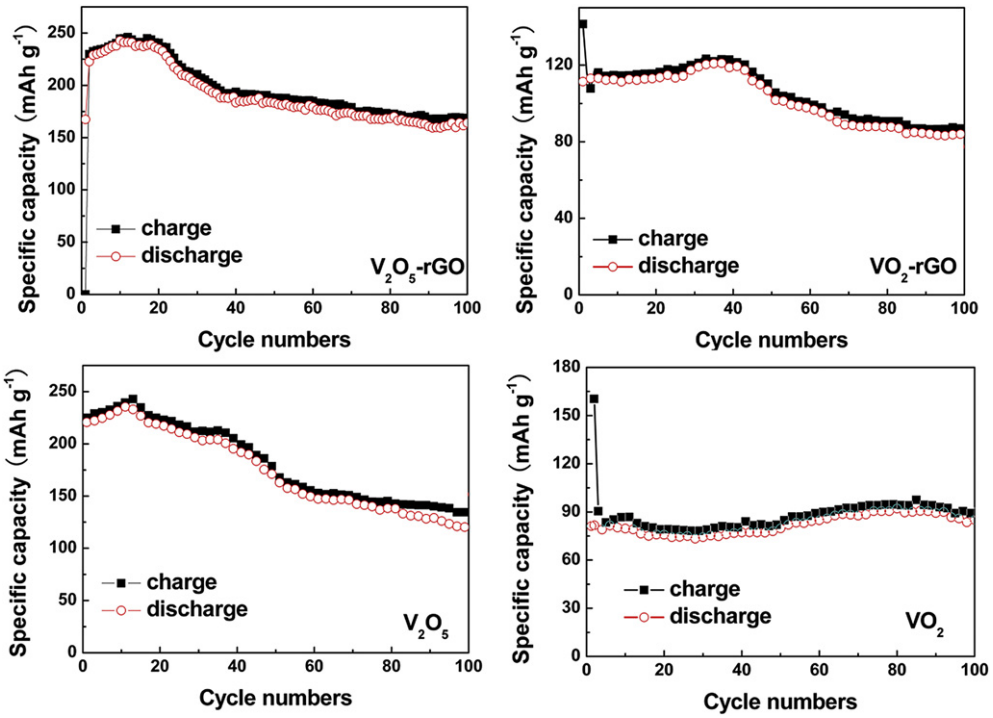

Fig. 8. The cycling performance of different vanadium oxides and their rGO modified hybrid electrodes during 100 cycles charge/discharge with current density of 20 mA g^{-1}.

voltage. Therefore, we think that VO_2 and VO_2–rGO are fitter for as capacitor materials other than lithium battery.

The combination of the layered structured graphene on the surface of vanadium oxides and the high reactivity of V_2O_5 or VO_2 with the Li ion in the conversion process provided a strong technological support for vanadium oxide in LIBs and non-aqueous SCPs. In case of V_2O_5–rGO, two pair of obvious oxidation/reduction peaks (P1/P1′ and P2/P2′) and a pair of small oxidation/reduction peaks (P3/P3′) were observed in the initial cathodic scan in the voltage window of 4.0 to 3.0 V, corresponding to the first Li

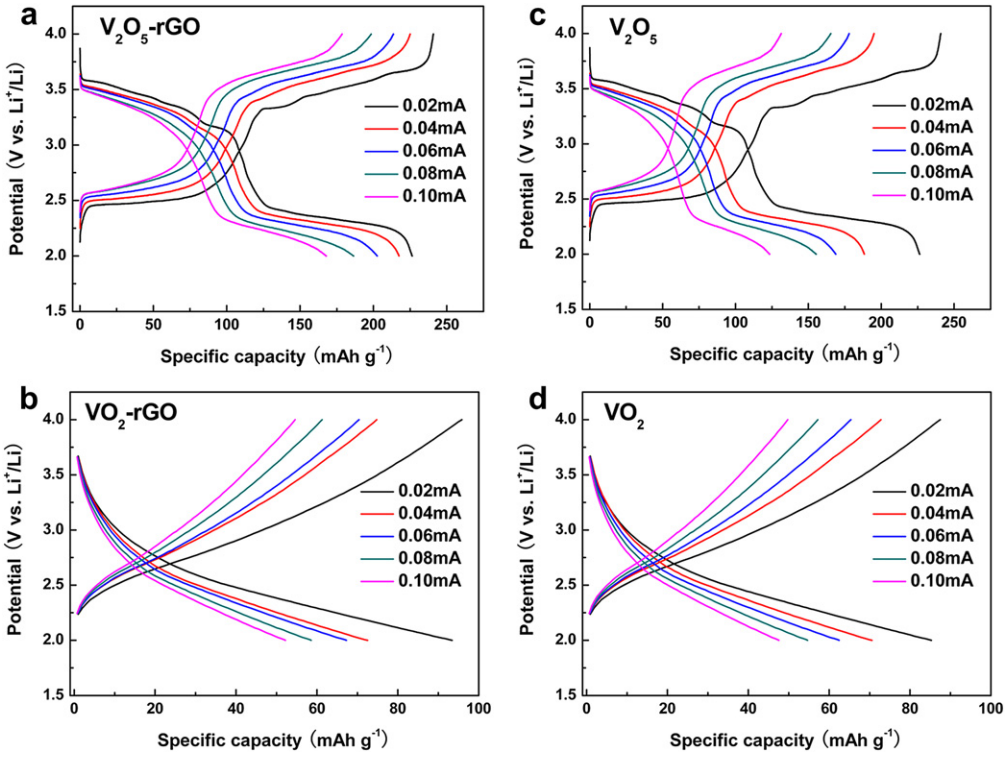

Fig. 9. C-rates performance of V_2O_5–rGO (a), VO_2–rGO (b), V_2O_5, (c) and VO_2 (d) as cathode materials.

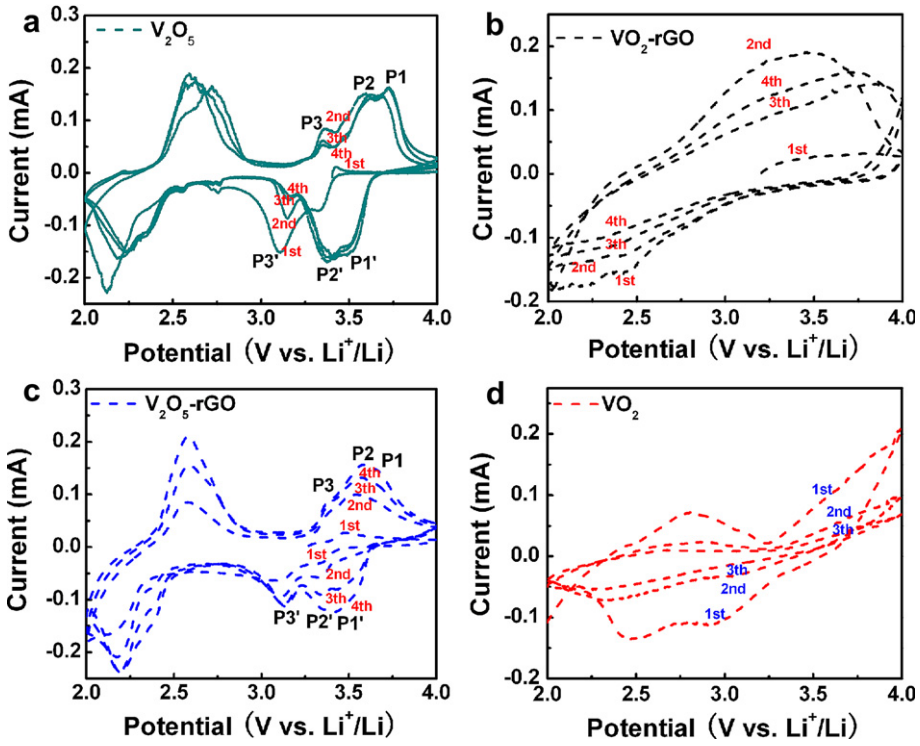

Fig. 10. CV curves of the synthesized electrode materials with scan speed of 0.1 mV s^{-1} in the voltage range of 2–4 V for the first three cycles.

insertion process in steps (Eq (3)). It need to be mentioned that the P3/P3′ peaks, which seldom were reported by former researcher, were observed at 3.0 V to 3.5 V, which maybe attributed to the special micro-nanostructure and good crystalline of V_2O_5 [50].

In addition, P1′ and P2′ peaks moved to higher voltage after three cycles scan and the peak voltage difference became small, therefore the reversibility was enhanced. Further to cathodic scan of the V_2O_5—rGO from 2.5 to 2.0 V, the peak appearing at 2.3 V reveals the second Li insertion process occurs as Eqs. (1) and (2). The oxidation/reduction peak in the voltage around 3.4 V should be considered to be the overlap of two oxidized/reduced peaks, which was ascribed to the micro-nanorod structure of the V_2O_5 [50]. To the best of our knowledge, it is the first time that the micro-nanosized V_2O_5—rGO composite has been achieved by hydrothermal reduction of GO on the surface of V_2O_5. The rGO effectively avoided aggregation and collapse of V_2O_5 and influenced the

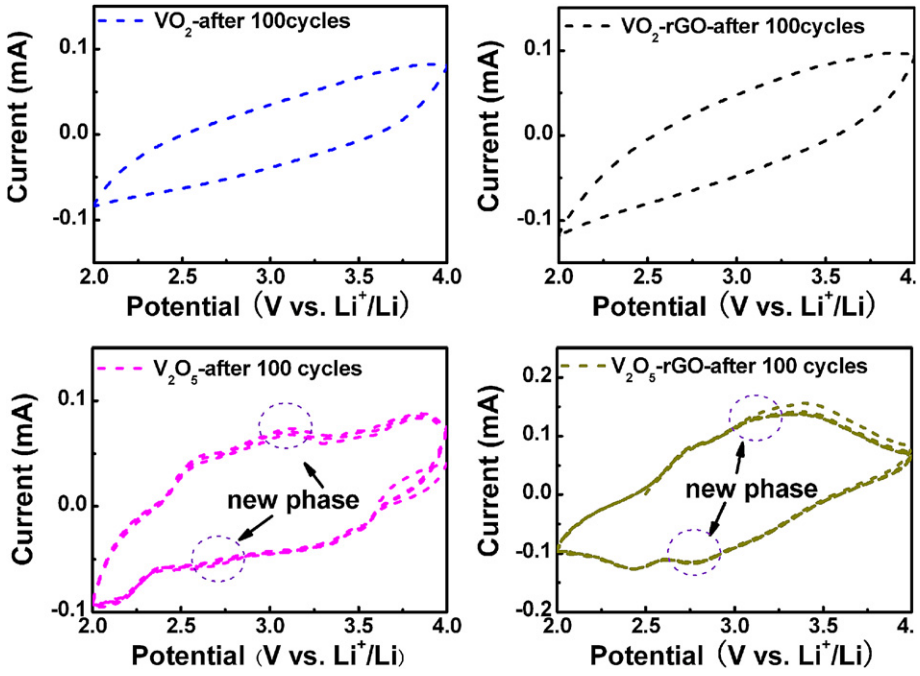

Fig. 11. CV curves of the synthesized electrode materials with scan speed of 0.1 mV s^{-1} in the voltage range of 2–4 V, after 100 cycles charge/discharge.

electrolyte diffusion process while charging/discharging. Especially, the complicated chemical process may result in some other reversible chemical reactions among surface-electrolyte species, thus it will make extra contributions to the enhanced electrochemical performance. Similar to that of pure VO_2 electrode, no obvious redox peaks were observed on the CV curves of VO_2–rGO composites. While the whole closed curve area of VO_2–rGO electrode was larger than that of pure VO_2, which indicated larger capacitance of VO_2–rGO.

The slow decay of capacity still could not be effectively avoided for the unstable structure of vanadium oxides and their lithiated species, even rGO was used as carbon coating layer. The capacity decay of V_2O_5 electrode at plateaus was almost equal proportionally, while a small plateaus occurred at the around of 2.5 V (Fig. 11) after 100 cycles charge/discharge process, which indicated the second Li insertion/extraction mechanism changed after longtime charge/discharge and a new crystal phase formed in this process. The cycle performance was not improved effectively by modifying the surface of vanadium oxide with rGO as carbon coating layer. Also, it was found that the amount of lithium intercalation/deintercalation was essential to control the cycling stability. As for VO_2–rGO electrode, the capacity decay is serious than that of pure VO_2 at the initial dozens of cycles. The reason maybe is attributed to that of the thickness of rGO layer on the surface of VO_2 is thin, which cannot play a role of elastic carbon shell to protect the collapse of VO_2 effectively. This result is corresponding to that of HRTEM images.

AC electronic impedance spectra (EIS) were also used to study the change of conductivity for vanadium oxides-Li cells at different electrochemical status. Before testing the impedances, the cells were charged or discharged at each constant voltage for 2 h. As shown in Fig. 12, one semicircle was observed during the charge

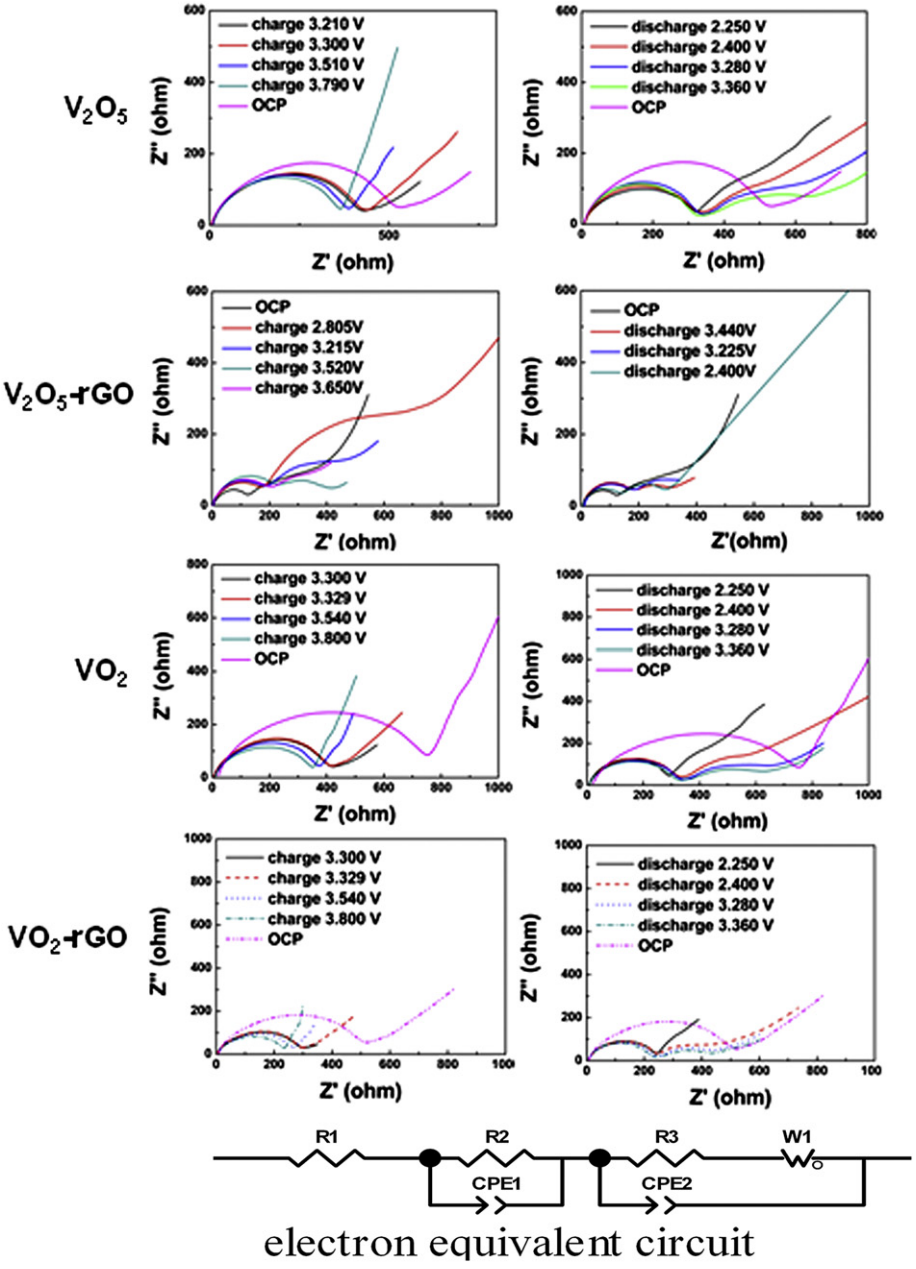

Fig. 12. AC impedance of the synthesized electrode materials at different electrochemical status.

process for VO_2, VO_2/rGO and V_2O_5 cells, while two semicircles were found for V_2O_5/rGO. Differently, during the discharge process from 4 V to 2 V, all the four electrodes have two semicircles. This result is similar with that of other layered cathode materials [51–53]. Usually, at ultrahigh frequency (>10 kHz), a point Ωic resistance (R1) is corresponding to the transport resistance of lithium ions and electron from electrolyte, membrane, conducting wire and active material particles. At high frequency, the semicircles are corresponding to the transport resistance of lithium ions from the insulating layer of active particle surface. At intermediate frequency, a semicircle is corresponding to the electron transport. At low frequency, an oblique line is corresponding to the solid transport of lithium ions in the active material. Based on this understanding, the electron equivalent circuit to analyze the EIS is given in Fig. 12. In this equivalent circuit, R1 refers to the uncompensated ohmic resistance between the working electrode and the reference electrode, R2 represents the resistance for lithium ion diffusion in the surface layer (including SEI layer and surface-modification layer), CPE1 is the constant phase-angle element depicting the non-ideal capacitance of the surface layer, R3 refers to the charge transfer resistance, W_o represents the Warburg impedance describing the lithium ion diffusion in the bulk material, and CPE2 is the constant phase-angle element depicting the non-ideal capacitance of the double layer. Among these parameters, R1, R3 and W_o can be used to quantify the polarization behaviors, i.e., ohmic polarization, activation polarization (also termed as charge transfer polarization), and diffusion polarization.

The obvious difference of impedance at different electrochemical status was observed, which should be attributed to the structure change of vanadium oxides and their lithiated species. As shown in Fig. 12, with the charge potential increased from open circuit potential (OCP) to 4 V, the lithium ions extracted from the lattice of lithiated species ($Li_2V_2O_5$ and LiV_2O_5). Two semicircles were observed on V_2O_5–rGO electrode, and the first semicircle became bigger and the second semicircle trended to smaller when charge potential rise. In the discharge process, the lithium ions inserted into the lattice of vanadium oxides and the first semicircle became smaller while the second semicircles became smaller. In case of V_2O_5, with the charge potential increased, the semicircle became small, while in the discharge process (from 4 V to 2 V), the second semicircle at intermediate frequency formed gradually. The first semicircle is relative unchanged and the second semicircle became too bigger. This indicated that the amount of lithium ions in the lattice of vanadium oxides cause the structure expending or contracting. As for cells with VO_2 and VO_2–rGO as cathode, only one semicircle at OCP was observed and its diameter became smaller with charge potential increased (lithium ion extracted from $LiVO_2$). While in the discharge process, lithium ions inserted in the lattice of VO_2. Another semicircle formed at intermediate frequency and its diameter became smaller from about 400 Ω to 200 Ω. This result also confirmed that the amount of lithium ion in the lattice of VO_2 affect their conductivity.

The enhanced capacity and improved cycling capacity up to 100 cycles of the V_2O_5–rGO micro-nanoscaled composite could be attributed to the following factors. First, as a result of the micro-nanoscaled topography of V_2O_5 obtained by CTAB hydrothermal reduction-heat treatment in air atmosphere, the charge/discharge capacity was improved after dozens of the charge/discharge cycles. Second, good interparticle electrical contact of vanadium oxides–rGO electrodes was kept and the usual drawbacks of nanoparticles such as poor active mass integrity and high surface reactivity were avoided. Finally, by introducing graphene to modify the surface of vanadium oxides, the collapse of active materials which occurred during longtime charge/discharge process was prevented partially. As for VO_2–rGO, the structure collapse in the high C-rates charge/discharge process was not serious because only one Li^+ ion insertion/extraction in VO_2 and the volumetric expansion is small. Besides, rGO plastic layer on the surface of VO_2 can effectively prevent the volume expansion of VO_2 during the Li^+ ions insertion/extraction process, thus the cycling performance of VO_2–rGO was better than that of pure VO_2 electrode.

4. Conclusion

In summary, novel vanadium oxide–rGO (V_2O_5–rGO and VO_2–rGO) hybrid cathode materials, of which are fabricated by thermic-reduced graphene coated on the surface of micro-nanosized vanadium oxide, have been successfully synthesized by a facile hydrothermal-low temperature pyrolysis approach. The obtained V_2O_5–rGO and VO_2–rGO composites can successfully be integrated into flexible storage devices such as lithium rechargeable batteries and supercapacitors. The capacity decay mechanism of V_2O_5 and V_2O_5–rGO composite was conjectured and the new pair of redox peak in CV curve at 3.1 V/2.75 V maybe is indirect evidence, which indicated new phase formed after one hundred cycles of charge/discharge and the initial redox peaks became unobvious, which also indicated that the amount of lithium ion intercalation/deintercalation was essential to control the cycling stability. The uniform coating of graphene around the surface of vanadium oxides ensures good close electrical contact, therefore higher specific capacity and enhanced cycling performance than pure VO_2 and V_2O_5 electrodes. Furthermore, the integration of other functional materials with a nanostructure graphene sheets could be used in various applications, such as fuel cell, photovoltaic cell, gas sensors, photocatalysis devices and organic synthesis.

Acknowledgment

We acknowledge the financial support from the National Natural Science Foundation of China (Grant No. 61071040), Leading Academic Discipline Project of Shanghai Municipal Education Commission (No. J50102) and Innovative Foundation of Shanghai University. We thank Instrumental Analysis and Research Center of Shanghai University. Thank Yamei Zhu (College of Foreign Language, Changchun Institute of Technology, Changchun, China) to polish the language.

References

[1] T.F. Yi, C.B. Yue, Y.R. Zhu, R.S. Zhu, X.G. Hu, Rare Metal Mat. Eng. 38 (2009) 1687–1692.
[2] A. Hayashi, Glass Technol. Part A 49 (2008) 213–220.
[3] E. Shembel, R. Apostolova, V. Nagirny, B. Markovsky, J. Power Sources 80 (1999) 90–97.
[4] B.V.R. Chowdari, M.V. Reddy, T. Yu, C.H. Sow, Z.X. Shen, C.T. Lim, G.V.S. Rao, Adv. Funct. Mater. 17 (2007) 2792–2799.
[5] H.K. Park, Solid State Ionics 176 (2005) 307–312.
[6] Z. Ying, Q. Wan, H. Cao, Z.T. Song, S.L. Feng, Appl. Phys. Lett. 87 (2005) 113108–113111.
[7] E. Frackowiak, A. Malak, K. Fic, G. Lota, C. Vix-Guterl, J. Solid State Electr. 14 (2010) 811–816.
[8] H. Kim, S.W. Kim, J. Hong, H.D. Lim, H.S. Kim, J.K. Yoo, K. Kang, J. Electrochem. Soc. 158 (2011) 930–935.
[9] Y.Q. Zou, Y. Wang, Nanoscale 3 (2011) 2615–2620.
[10] Q.Y. Lai, J.H. Huang, J.M. Song, L.M. Chen, X.Y. Ji, Chin. J. Inorg. Chem. 23 (2007) 237–242.
[11] J. Chen, F.Y. Cheng, J. Mater. Chem. 21 (2011) 9841–9848.
[12] T. Kudo, Y. Ikeda, T. Watanabe, M. Hibino, M. Miyayama, H. Abe, K. Kajita, Solid State Ionics 152 (2002) 833–841.
[13] P. Cui, Z.J. Jia, L.Y. Li, T. He, Electrochim. Acta 56 (2011) 4571–4575.
[14] Y. Wang, K. Takahashi, K. Lee, G.Z. Cao, Adv. Funct. Mater. 16 (2006) 1133–1144.
[15] A. Manthiram, A.M. Kannan, Solid State Ionics 159 (2003) 265–271.
[16] N. Asim, S. Radiman, M.A. Yarmo, M.S.B. Golriz, Micropor. Mesopor. Mat. 120 (2009) 397–401.
[17] Z.S. Chao, E. Ruckenstein, Chem. Mater. 14 (2002) 4611–4618.

[18] Y.T. Qian, X.Y. Chen, X. Wang, Z.H. Wang, J.X. Wan, J.W. Liu, Nanotechnology 15 (2004) 1685–1687.
[19] C. Vijayan, M.R. Parida, C.S. Rout, C.S.S. Sandeep, R. Phiip, P.C. Deshmukh, J. Phys. Chem. C 115 (2011) 112–117.
[20] M.S. Whittingham, N.A. Chernova, M. Roppolo, A.C. Dillon, J. Mater. Chem. 19 (2009) 2526–2552.
[21] G.Z. Cao, K. Takahashi, Y. Wang, J. Phys. Chem. B 109 (2005) 48–51.
[22] G.Z. Cao, Y. Wang, K. Takahashi, H.M. Shang, J. Phys. Chem. B 109 (2005) 3085–3088.
[23] J.H. Harreld, B. Dunn, L.F. Nazar, Int. J. Inorg. Mater. 1 (1999) 135–146.
[24] S. Kuwabata, S. Masui, H. Tomiyori, H. Yoneyama, Electrochim. Acta 46 (2000) 91–97.
[25] S. Kuwabata, M. Tomiyori, J. Electrochem. Soc. 149 (2002) A988–A994.
[26] G.R. Goward, L.F. Nazar, F. Leroux, Electrochim. Acta 43 (1998) 1307–1313.
[27] N. Asim, S. Radiman, M.A. Yarmo, Mater. Lett. 62 (2008) 1044–1047.
[28] I. Stojković, N. Cvijetićanin, S. Mentus, Russ. J. Phys. Chem. A 85 (2011) 2344–2348.
[29] C. Cai, Y. Wang, Materials 2 (2009) 1205–1238.
[30] L.J. Zhi, M.H. Liang, J. Mater. Chem. 19 (2009) 5871–5878.
[31] G.X. Wang, X.P. Shen, J. Yao, J. Park, Carbon 47 (2009) 2049–2053.
[32] C.Y. Wang, Y. Wang, Z.Q. Shi, Y. Huang, Y.F. Ma, M.M. Chen, Y.S. Chen, J. Phys. Chem. C 113 (2009) 13103–13107.
[33] W.C. Ren, Z.S. Wu, L. Wen, L.B. Gao, J.P. Zhao, Z.P. Chen, G.M. Zhou, F. Li, H.M. Cheng, ACS Nano. 4 (2010) 3187–3194.
[34] L.L. Zhang, X.S. Zhao, R. Zhou, J. Mater. Chem. 20 (2010) 5983–5992.
[35] J.P. Tu, Y.J. Mai, X.L. Wang, J.Y. Xiang, Y.Q. Qiao, D. Zhang, C.D. Gu, Electrochim. Acta 56 (2011) 2306–2311.
[36] Y.G. Guo, B. Wang, X.L. Wu, C.Y. Shu, C.R. Wang, J. Mater. Chem. 20 (2010) 10661–10664.
[37] X.P. Shen, Z.Y. Ji, J.L. Wu, H. Zhou, H.T. Xi, J. Mater. Sci. 46 (2011) 1190–1195.
[38] Y. Cui, H.L. Wang, L.F. Cui, Y.A. Yang, H.S. Casalongue, J.T. Robinson, Y.Y. Liang, H.J. Dai, J. Am. Chem. Soc. 132 (2010) 13978–13980.
[39] X.L. Cui, X.Y. Zhang, H.P. Li, Y.H. Lin, J. Mater. Chem. 20 (2010) 2801–2806.
[40] I. Honma, S.M. Paek, E. Yoo, Nano. Lett. 9 (2009) 72.
[41] S.B. Yang, G.L. Cui, S.P. Pang, Q. Cao, U. Kolb, X.L. Feng, J. Maier, K. Mullen, Chemsuschem 3 (2010) 236.
[42] H.Q. Cao, B.J. Li, J. Shao, G.Q. Li, M.Z. Qu, G. Yin, Inorg. Chem. 50 (2011) 1628.
[43] Y.F. Tang, F.Q. Huang, H. Bi, Z.Q. Liu, D.Y. Wan, J. Power Sources 203 (2012) 130.
[44] C.M. Li, Y. Wang, C.X. Guo, J.H. Liu, T. Chen, H.B. Yang, Dalton T. 40 (2011) 6388.
[45] E. Barrado, R. Pardo, Y. Castrillejo, M. Vega, J. Electroanal. Chem. 427 (1997) 35.
[46] Y. Zhang, X. Liu, G. Xie, Mater. Sci. Eng. B 175 (2010) 164.
[47] J. Mendialdua, R. Casanova, Y. Barbaux, J. Electron. Spectrosc. 71 (1995) 249.
[48] Y. Chen, K. Xie, Z.X. Liu, Appl. Surf. Sci. 133 (1998) 221.
[49] J. Mendialdua, R. Casanova, Y. Barbaux, An. Quim. Int. 94 (1998) 13.
[50] A.Q. Pan, J.G. Zhang, Z.M. Nie, G.Z. Cao, B.W. Arey, G.S. Li, S.Q. Liang, J. Liu, J. Mater. Chem. 20 (2010) 9193.
[51] J. Liu, Q.Y. Wang, B. Reeja-Jayan, A. Manthiram, Electrochem. Comm. 12 (2010) 750.
[52] J. Liu, A. Manthiram, J. Mater. Chem. 20 (2012) 3961.
[53] M. Koltypin, V. Pol, A. Gedanken, D. Aurbach, J. Electrochem. Soc. 154 (2007) 605.